Optics and Laser Technology 128 (2020) 106227

Contents lists available at ScienceDirect

Optics and Laser Technology

journal homepage: www.elsevier.com/locate/optlastec

Femtosecond laser direct written off-axis fiber Bragg gratings for sensing applications

Duarte Viveiros[a,b,*], Vítor A. Amorim[a,b], João M. Maia[a,b], Susana Silva[a,b], Orlando Frazão[a,b], Pedro A.S. Jorge[a,b], Luís A. Fernandes[c,1], Paulo V.S. Marques[a,b]

[a] Centre for Applied Photonics, INESC TEC, 4150-179 Porto, Portugal
[b] Department of Physics and Astronomy, Faculty of Science, University of Porto, 4169-007 Porto, Portugal
[c] OZ Optics, Ottawa, Ontario K0A 1L0, Canada

HIGHLIGHTS

- Femtosecond laser direct writing of first-order off-axis FBGs in an SMF-28e fiber.
- The minimum FBG inscription offset of 2.5 μm to create a multimode section found.
- The impact of the fabrication parameters in the number of supported modes and birefringence studied.
- The multimode section as sensing head for strain, temperature, and curvature sensing explored.

ARTICLE INFO

Keywords:
Birefringence
femtosecond laser direct writing
off-axis fiber Bragg gratings
optical fiber sensors
single mode fiber

ABSTRACT

First order off-axis fiber Bragg gratings (FBGs) were fabricated in a standard single mode fiber (SMF-28e) through femtosecond laser direct writing. A minimum offset distance between the grating and core center of 2.5 μm was found to create a multimode section, which supports two separate fiber modes ($LP_{0,1}$ and $LP_{1,1}$), each split into two degenerate polarization modes. The resulting structure breaks the cylindrical symmetry of the fiber, introducing birefringence ($\approx 10^{-4}$) resulting in a polarization dependent Bragg wavelength for each mode. Based on the modal and birefringence behavior, three off-axis FBGs were fabricated with 3.0, 4.5 and 6.0 μm offsets from the core center, and then characterized in strain, temperature, and curvature. The tested off-axis FBGs exhibited a similar strain sensitivity of ~1.14 pm/με and a temperature sensitivity of ~12 pm/C. The curvature and orientation angle were simultaneously monitored by analyzing the intensity fluctuation and the wavelength shift of the $LP_{1,1}$ Bragg resonance. A maximum curvature sensitivity of 0.53 dB/m^{-1} was obtained for the off-axis FBG with a 3.0 μm offset.

1. Introduction

Fiber Bragg gratings (FBGs) are important and invaluable passive optical devices in optical communication, sensing, and fiber laser applications. Their most distinguishing feature is the flexibility they offer for achieving specific spectral characteristics, due to the broad range of variation in their physical parameters (induced index change, length, apodization, period chirp, and fringe tilt) [1,2]. FBGs can be conventionally photo-inscribed into the core of a standard single mode fiber (SMF) using ultraviolet (UV) laser exposure through a phase mask or by holographic methods, which allows the inscription of a single FBG only in a portion of the fiber core [3,4]. Since the demonstration of FBG inscription using femtosecond (fs) laser technology [5], this technique has been explored in different types of optical fibers, including in coreless fibers [6]. The underlying non-linear light-matter interaction opens the possibility to inscribe gratings not only in the core, but also in the fiber cladding with high spatial resolution [7]. The fs-laser direct writing technique used in this paper [2,8,9] has a few advantages relatively to techniques that employ a phase mask, either by UV exposure [3,4] or by non-direct writing fs-laser exposure [7]. With the present

* Corresponding author.
E-mail addresses: carlos.d.viveiros@inesctec.pt (D. Viveiros), vitor.a.amorim@inesctec.pt (V.A. Amorim), joao.m.maia@inesctec.pt (J.M. Maia), susana.o.silva@inesctec.pt (S. Silva), ofrazao@inesctec.pt (O. Frazão), pedro.jorge@fc.up.pt (P.A.S. Jorge), luisfernandes@luisfernandes.org (L.A. Fernandes), psmarque@fc.up.pt (P.V.S. Marques).
[1] Currently with VIAVI Solutions, Ottawa, Ontario K2J 0P7, Canada.

https://doi.org/10.1016/j.optlastec.2020.106227
Received 18 December 2019; Received in revised form 17 March 2020; Accepted 21 March 2020
0030-3992/ © 2020 Elsevier Ltd. All rights reserved.

technique there is no need for phase mask or hydrogen loading, and it has excellent design flexibility, enabling rapid change of grating parameters, such as length, bandwidth, or Bragg wavelength [10].

FBGs can be employed as optical sensors to measure physical parameters, such as temperature [11], strain [12], curvature/bending [13,14], pressure [15], or twist [16] either individually or simultaneously [17], through wavelength monitoring or power detection [18]. Sensing configurations involving the fabrication of birefringent FBGs [19], tilted FBGs [20], FBG arrays [10] or sampled FBGs [11] have already been demonstrated. Similar bending sensors have also been shown in depressed cladding fibers [21], in few-mode fibers [22] and in twin-core few-mode fibers [23], which showcases the versatility of this technique. One of the issues with common FBG sensing configurations is the low sensitivity to curvature, given that the fiber mode is strongly confined to the core and is only slightly influenced by the external bending. A possible way to solve this is to employ cladding modes [17,23,24]. However, when utilizing cladding modes, a suitable coupling mechanism is imposed to recouple the mode back into the core, to allow remote interrogation with low loss [12,18]. This can be done through offset splicing [26], core mismatching [25] or abrupt taper [25] which, nevertheless, brings up issues of low reproducibility (offset splicing), weakened mechanical strength (abrupt taper), and complex fabrication processes [18].

In this work, we demonstrate the production of first order off-axis FBGs in an SMF-28e through fs-laser direct writing. First, we optimized the fabrication of off-axis FBGs, and characterized the grating spectra while varying the lateral distance of the grating to the core center. For distances equal or above 2.5 μm, we observed a multimode section in the SMF-28e that can support two-mode ($LP_{0,1}$ and $LP_{1,1}$) FBGs, similarly to what was already observed by other [7,26,27]. The influence of the lateral offset to strain, temperature and curvature sensing is investigated, by fabricating three FBGs, with offsets of 3.0, 4.5 and 6.0 μm. This novel fabricated device presents some advantages like small fabrication complexity, reduced splicing loss, and low transmission loss. The existence of two separate fiber modes, each split into two degenerate polarization modes, induced by the larger asymmetric structure formed during the writing process, also enables simultaneous detection of multiple parameters.

2. Manufacturing procedures

A laser direct writing system was employed in the fabrication of off-axis FBGs inside standard single mode optical fibers (SMF-28e, Corning). The writing system uses a fiber amplified fs-laser (Satsuma HP, from Amplitude Systèmes) providing a second harmonic beam at 515 nm, with a pulse duration of ~250 fs at a repetition rate of 500 kHz. The orientation of the linearly polarized beam was set parallel to the scanning direction. The laser beam was focused inside the fiber core with a 100× oil immersion lens (Olympus PLN 100XO), 1.25 numerical aperture, which is mounted on a Y (Newport M-ILS150CC) and Z (Newport VP-25XA) precision linear stages. In this system, the X air-bearing linear stage (ABL10100-LN) is the scanning direction and is parallel to the fiber axis, Y is the direction transversal to the fiber axis and Z is the beam propagation direction. The optical fiber coating is removed and carefully cleaned using ethanol. The bare fiber is then clamped to two three-axis positioners (MBT616/M, Thorlabs) that are mounted on the X air-bearing linear stage. The fiber is immersed in an index matching liquid (Cargille cat#19571, RI = 1.4587) to eliminate the cylindrical aberration, due to the fiber geometry, and to compensate for the refractive index (RI) mismatch at the surface of the optical fiber. The optical fiber is imaged through the writing objective onto a CCD camera, allowing precise positioning of the Bragg grating on the fiber core. The real-time monitoring and the adjustment of the fabrication tension are done through a previously calibrated load cell (Interface SML series). The tension is applied by increasing the distance between the two 3-axis positioners, which are connected to the load cell. The fiber is kept under tension (1 N) to remove the curvature during the writing process and to ensure that remains in position.

During writing, the laser gate was externally controlled by a periodic square function with a duty cycle of 50% generated by a synthesized function generator (DS345, Stanford Research Systems). This simple arrangement allows the automated writing of gratings by simply translating the optical fiber at constant velocity (v) along X, with the signal modulation turned on; the Bragg wavelength can easily be tuned by the adjustment of the modulation frequency, f_{mod}. The Bragg wavelength is given by the Bragg relation $\lambda_B = 2n_{eff}\frac{v}{f_{mod}}$, where is the effective refractive index of the guided mode. More details regarding the alignment and writing processes were previously published by the authors [29].

To test the devices, a broadband light source (model ASE2000), ranging from 1545 to 1555 nm was injected on the fiber through an optical circulator. The spectrum was measured in either reflection or transmission with an optical spectrum analyzer (OSA, model Yokogawa AQ6370D) with a resolution of 0.02 nm. The signal is measured without polarization control. All spectra are normalized to the transmitted spectrum of the light source.

3. Experimental results and discussion

A. Characterization of the writing process

In order to measure the RI modifications induced by the fs-laser, five waveguides were written with different pulse energies and scanning velocities, as represented in Table 1.

Fig. 1 shows an optical microscope view of the cross-section of the waveguiding structures (a), and the respective refractive index profile (b), which was measured at 980 nm with an IFA-100 (Interfiber Analysis) interferometric system [30]. The RI modification has an asymmetric shape and is composed by a region of reduced refractive index (shown in blue) located above a region of increased refractive index (shown in red). The RI contrast was seen to increase with pulse energy ranging from 60 to 120 nJ, evolving from $\approx 0.5 \times 10^{-1}$ to $\approx 1.0 \times 10^{-2}$ and from $\approx 1.4 \times 10^{-2}$ to $\approx 2.2 \times 10^{-2}$ for the bottom and top regions, respectively. The contrast achieved inside the optical fiber core is similar to those mentioned seen in the cladding. The height of the modification structures grows with the increase of the pulse energy, extending from 7.5 to 11 μm, with the width maintaining at ≈3 μm. Velocities ranging from 100 to 200 μm/s show no significant impact on the RI modification. The IFA measurements of the RI profile suggest that the induced modifications are in the Type-I regime [31].

B. Fabrication of off-axis FBGs

The fabrication of the FBGs with an offset from the core center was performed by taking advantage of the high precision optical fiber positioning system (Y stage), as proven by Fig. 1. The grating period and length were defined to be 535.44 nm and 15 mm, respectively. The optimal writing conditions for an FBG centered in the core were found to be 60 nJ of pulse energy, 50 μm/s of scanning velocity, fiber tension of 1 N, and a writing beam polarization aligned with the scanning direction of the fiber, [29]. The fabrication of the off-axis FBGs with 1 N of tension introduces birefringence possibly via elastooptic index change [19], as shown in Fig. 2. The fundamental Bragg resonance splits into two peaks, when relaxing the optical fiber. The optimum pulse energy to write off-axis FBGs was found to be 140 nJ, instead of 60 nJ, as it will improve the 2nd mode reflectivity.

Table 1
Writing parameters of the fs-laser written WGs.

Waveguides (WGs)	1	2	3	4	5
Pulse energy (nJ)	90	90	90	60	120
Write velocity (μm/s)	100	200	200	100	100

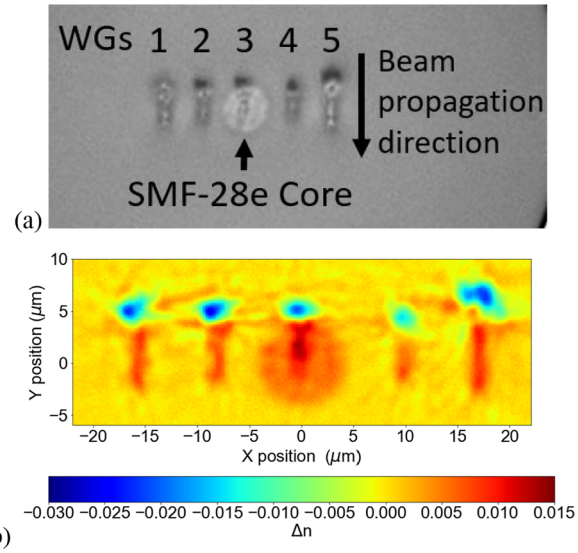

Fig. 1. Fs-laser written waveguides inside a SMF-28e fiber: (a) cross-section and (b) refractive index profile.

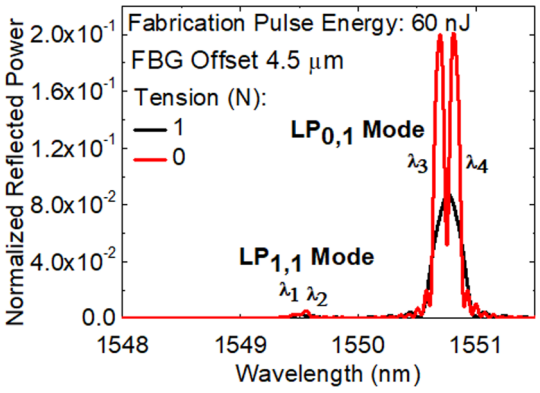

Fig. 2. Off-axis FBG with 4.5 μm offset from the core center fabricated with 60 nJ pulse energy.

Fig. 3 shows off-axis FBGs fabricated with 3.0, 4.5 and 6.0 μm offsets from the core center. The fabrication method gives full control of where the grating is inscribed: it can be inscribed totally inside the core, over the core-cladding boundary or totally outside of the fiber core. Analyzing the top and end view section images presented in Fig. 3, it is possible to verify the increase of the core effective size in the section where the FBG is inscribed.

Fig. 4 (a) and (b) shows the transmitted and reflected spectra of the off-axis FBGs written with an offset distance of 3.0, 4.5 and 6.0 μm. The transmission spectra presented in Fig. 4 (a) consists of two bands: two Bragg resonance with two peaks, due to birefringence induced by the asymmetric structure, and several cladding mode resonances on the short wavelength side. From the reflection spectra shown in Fig. 4 (b), the existence of the Bragg resonance associated with the $LP_{1,1}$ mode is clearly visible.

To understand the effect of the off-axis FBGs inscribed in the SMF-28e, it is considered the V-number that determines: the number of modes supported by a fiber, the cutoff condition of the various modes and the respective propagation constants. This parameter is given by [32]:

$$V = \frac{2\pi a}{\lambda}\sqrt{n_{core}^2 - n_{clad}^2} \quad (1)$$

where a is the core radius, and n_{core} and n_{clad} are the refractive indices of the core and cladding, respectively. When the V-number is lower than 2.405 only one mode ($LP_{0,1}$) can propagate along the fiber at the wavelength λ. In the wavelength region of interest ($\approx$ 1550 nm), the SMF-28e fiber only supports the fundamental mode $LP_{0,1}$, i.e. the fiber is single mode [33]. As can be seen from Figs. 1 and 3, when inscribing the off-axis grating, the core size and its refractive index increases, which results in an increase of the V-number. If we take typical values (core index of 1.444 + 0.006, cladding index of 1.444, and core radius of 5.6 μm, for a grating inscription offset of 6.0 μm) we can estimate a V-number of ~2.991 at 1550.8 nm, which is above the cut-off condition. Therefore, the fiber section where the off-axis FBG is written turns into a two-mode fiber that can theoretically support the linearly polarized modes $LP_{0,1}$, and $LP_{1,1}$, explaining the additional resonance peak of the $LP_{1,1}$ mode observed in Fig. 4(b) [32]. With the increase of the offset from the core center, the grating reflectivity decreases, as can also be seen in Fig. 4 (b). For the off-axis FBGs with greater offset, the reflectivity can be improved by increasing the grating length. The estimated V-number was utilized to calculate the effective refractive index, n_{eff} through the modal dispersion (i.e., bV) curves reported in [32]. For a V-number of ~2.991, the correspondent b value for the modes $LP_{0,1}$, and $LP_{1,1}$ are 0.65 and 0.15, respectively. Accordingly, the estimated n_{eff} for the modes, $LP_{0,1}$, and $LP_{1,1}$ are ~1.448 and ~1.445, respectively. The Bragg relation was also used to determine the effective refractive index of the guided modes, resulting in a n_{eff} for the modes $LP_{0,1}$, and $LP_{1,1}$ of ~1.447 and ~1.446, respectively. It was considered the Bragg wavelength of each mode for the writing period of 535.44 nm. Thus, the estimated n_{eff} values, calculated through the two methods, present a good approximation.

The theoretical calculation was supported through a 2D analysis of the optical fiber structure and the electromagnetic field modes using the mode analysis of the COMSOL Multiphysics®. A structure similar to the presented in the inset of Fig. 3 (d) for the fabricated off-axis FBG with 6.0 μm from the core center was designed. The correspondent RI values were defined through the IFA measurements of the RI profile presented in Fig. 1 (b). The electric field distribution, E_z, in 2D (V/m) of the $LP_{0,1}$ and $LP_{1,1}$ modes in the core diameter at a wavelength of 1550 nm was evaluated, as shown in Fig. 5 (a) and (b), respectively.

The increase in core dimensions due to the off-axis FBG inscription affects the modal structure of the fiber, as observed in the intensity of the electric field for the $LP_{0,1}$ and $LP_{1,1}$ modes, yielding effective mode indices of ~1.4458 and ~1.444, respectively. The results achieved with the COMSOL Multiphysics® allows confirmation of the multimode propagation in the fiber section where the off-axis FBG is inscribed.

Fig. 6 shows the wavelength shift (a) and the birefringence (b) of the off-axis FBGs as a function of the offset distance. From Fig. 6 (b), it is observed that for lateral shifts above 2.0 μm, the Bragg resonance (for each mode) presents two peaks due to laser-induced birefringence. Fig. 6 (a) also shows that, with the increase of the offset distance, the Bragg wavelength of the $LP_{1,1}$ mode increases, while the Bragg wavelength of the $LP_{0,1}$ mode stays constant. This can be explained by the increase of the core's size with the offset distance (visible in Fig. 3), which leads to an increase of the V-number and, consequently, of the effective refractive index. For an offset higher than 7.5 μm, the off-axis FBG is undetected in both the transmission and reflection spectra. This means that the overlap between the core mode and the induced modification is negligible, resulting in a very weak Bragg reflected signal.

Due to the lateral offset inscription process and the asymmetric RI modification, the fs-laser writing process introduces birefringence to the SMF-28e, which causes the splitting of the Bragg resonance into two polarization modes [19]. The different Bragg resonance peak associated with each polarization axis can be used as a means to determine the degree of birefringence using the following equation [34]:

$$\Delta n_B = \frac{\lambda_{B2} - \lambda_{B1}}{2\Lambda} \quad (2)$$

For the FBG written with an offset of 4.5 μm, the two Bragg resonances of each mode ($LP_{1,1}$ and $LP_{0,1}$) are separated by 139 and

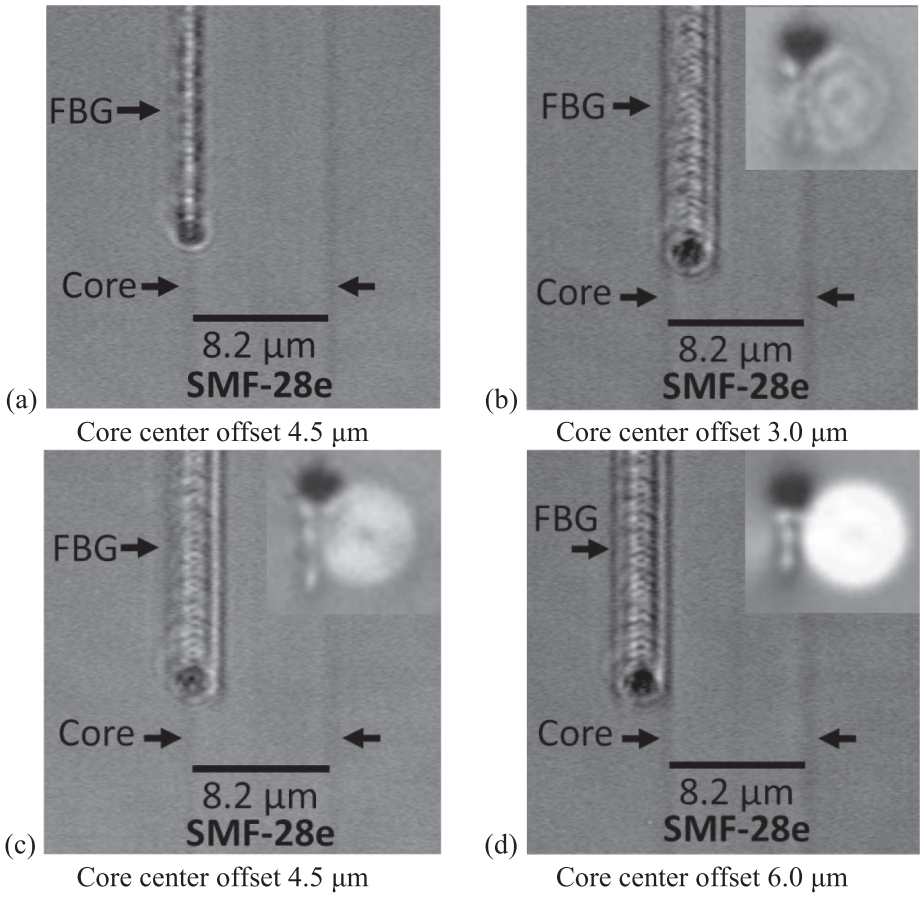

Fig. 3. Top-view images of the off-axis FBGs with an offset of: (a) 4.5 μm written with 60 nJ pulse energy and (b) 3.0 μm; (c) 4.5 μm; and (d) 6.0 μm written with 140 nJ pulse energy (insets: end-view optical micrographs). All gratings were written at 50 μm/s.

181 pm, yielding a birefringence value equal to 1.3×10^{-4} and 1.7×10^{-4}, respectively. It was also confirmed that vertically polarized incident light stimulates the Bragg resonances λ_4 and λ_2 from the $LP_{0,1}$ and $LP_{1,1}$ modes, respectively. In the case of horizontally polarized light, the corresponding Bragg resonances observed are λ_3 and λ_1 from the $LP_{0,1}$ and $LP_{1,1}$ modes, respectively. Fig. 6 (b) shows that, for the $LP_{0,1}$ mode, the birefringence decreases from a mean value of 1.91×10^{-4} to 1.62×10^{-4} (variation of 0.29×10^{-4}) when the offset distance increases from 2.5 to 6.5 μm. The birefringence of the $LP_{1,1}$ mode, decreases from 1.51×10^{-4} to 1.29×10^{-4} mean value (a difference of0.22×10^{-4}). The birefringence value of the FBG with a 7.5 μm offset is lower compared with the all the others. For an offset smaller than 2 μm the birefringence value is below the measurement resolution. These differences in the birefringence values may be due to small variations of the physical length and/or refractive index modulation of the grating, and also due to the differences in the strength of the gratings.

C. Off-axis FBGs for optical sensing

Three off-axis FBGs fabricated with 3.0, 4.5 and 6.0 μm offsets, were characterized in strain, temperature, and bending. Three test setups were developed for each measurement parameter. The results of the spectral variations with each measurand and for each device are presented.

D. Strain measurements

Each off-axis FBG was subjected to mechanical strain, by gluing one extreme of the optical fiber to a micro-positioning stage, while the other

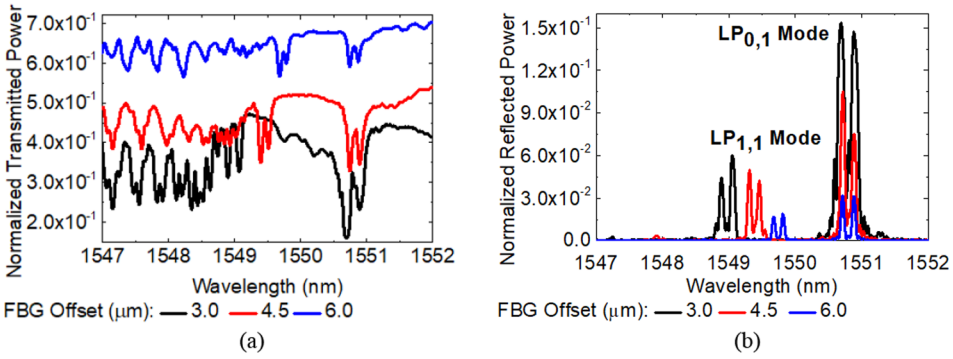

Fig. 4. Fs-laser off-axis FBGs: (a) transmission and (b) reflection spectra.

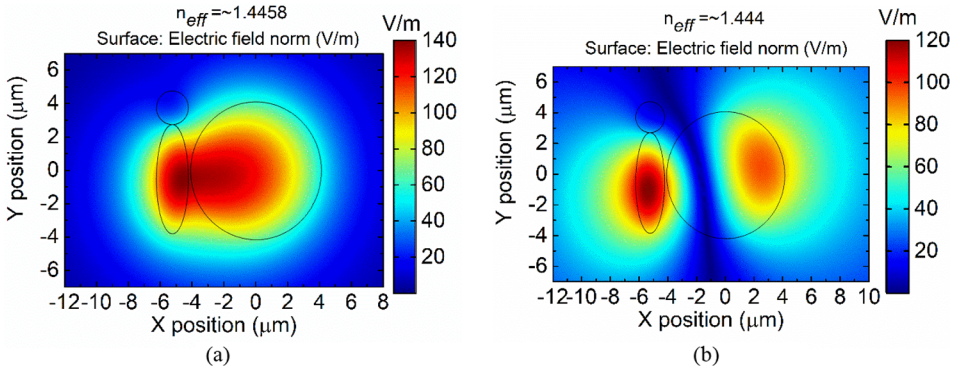

Fig. 5. Simulated intensity of the electric field at the core/structure for the: (a) $LP_{0,1}$ mode and (b) $LP_{1,1}$ mode.

side was glued to a fixed holder. The off-axis FBGs were stretched from 0 to 522 με in intervals of 43.5 με; the measurements were made at room temperature (~23 °C). Some of the acquired reflection spectra of the 6.0 μm offset FBG for different strain values are shown in Fig. 7 (a).

For this off-axis FBG, the reflection spectra evolution was recorded both during the fiber strain increase and decrease. When the fiber is stretched, there is a shift in the Bragg wavelength mainly due to changes in the grating period. For the FBG shown in Fig. 7 (a), the two Bragg resonances of each mode ($LP_{1,1}$ and $LP_{0,1}$) red-shifted by ~600 pm at the maximum applied strain, corresponding to a linear sensitivity of ~1.15 ± 0.01 pm/με. In addition, no hysteresis was observed. Similar sensitivities of ~1.13 ± 0.01 pm/με and ~1.16 ± 0.01 pm/με were achieved for each Bragg resonance of the 3.0 and 4.5 μm off-axis FBGs, respectively. These results are summarized in Table 2. The strain sensitivities obtained are similar to the sensitivities reported in this paper [13,34], which is 1.15 pm/με at 1550 nm wavelength. The amplitude of the two Bragg resonances of the two $LP_{1,1}$ and $LP_{0,1}$ modes are approximately constant with the applied strain for each off-axis FBG.

E. Temperature measurements

The temperature characterization of the three off-axis FBGs was performed simultaneously, and for that, the corresponding optical fibers were introduced in a tubular oven (Termolab) while being subjected to a constant strain of 66.7 με. The temperature of the oven was increased from 23 to 300 °C in steps of ~20 °C, for a dwell time of 5 min each. The cooling process to room temperature was done following the same protocol.

During this procedure, the grating spectra were recorded and some of the acquired reflection spectra of the off-axis FBGs with 3.0 and 6.0 μm offset are shown in Fig. 8.

The two Bragg resonances of each mode of the off-axis FBGs with 3.0 μm red-shifted by ~3.3 nm when subjected to a maximum temperature of 300 °C and showed a similar linear sensitivity of 12 pm/°C, as presented in Fig. 8 (b). The measured sensitivities are presented in Table 3; in summary, a linear sensitivity of ~12 ± 0.2 pm/°C was achieved for each Bragg resonance of each off-axis FBGs characterized. In addition, a negligible hysteresis was observed. For the sensitivity measurement of the off-axis FBG with a 6.0 μm offset, a temperature range from 22 to 200 °C was utilized.

These results are similar to the temperature sensitivity of the FBGs fabricated in the core of an SMF, which is 10.6 pm/°C at 1550 nm wavelength, [9,27]. The temperature variation has two effects over the Bragg wavelength shift given by [35]:

$$\frac{d\lambda_B}{dT} = \lambda_B a_L + \frac{\lambda_B}{n}\frac{dn}{dT} \tag{3}$$

where $d\lambda_B/dT$ is the temperature sensitivity of the FBG, a_L is the linear thermal expansion coefficient and dn/dT is the thermo optic effect in the waveguide mode. The first effect corresponds to the first term, increasing the reflected wavelength with temperature, while the second term reflects the thermo optic effect, which changes the refractive index of the waveguide mode with temperature [35].

For the off-axis FBG with 3.0 μm offset, the amplitude of the two Bragg resonances of both modes remain unchanged for the range of temperatures tested. For the off-axis FBG with a 4.5 μm offset, the results were very similar. Type I FBGs are known to be thermally stable up to ~300 °C when written within the fiber core center [29]; off-axis FBG fabricated with a 3.0 μm offset have a similar behavior as can be seen in Fig. 8 (a). In the case of the off-axis FBG with a 6.0 μm offset, however, the resonance amplitude decreases with the temperature increase, as can be seen in Fig. 8 (c). When the temperature reaches 240 °C the reflection spectra of the FBG becomes deformed, with the two Bragg resonances, for each mode, being poorly resolved. After heating up to 300 °C, the grating was cooled down to room temperature, and, during this process, the normalized reflected power increases as seen in Fig. 8 (d) at a temperature of 278.5 °C. This effect can be associated with the position of the FBG relative to the fiber core and with the heating process. For the off-axis FBG with 6.0 μm offset, the

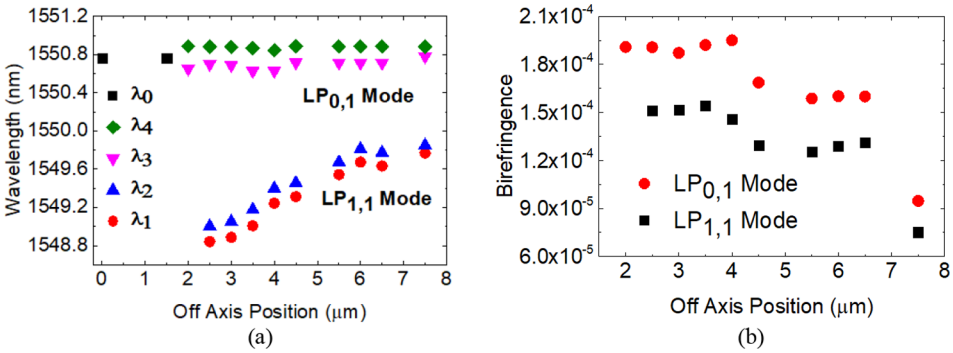

Fig. 6. Off-axis FBGs: (a) wavelength shift and (b) birefringence, as a function of the grating inscription position from core center.

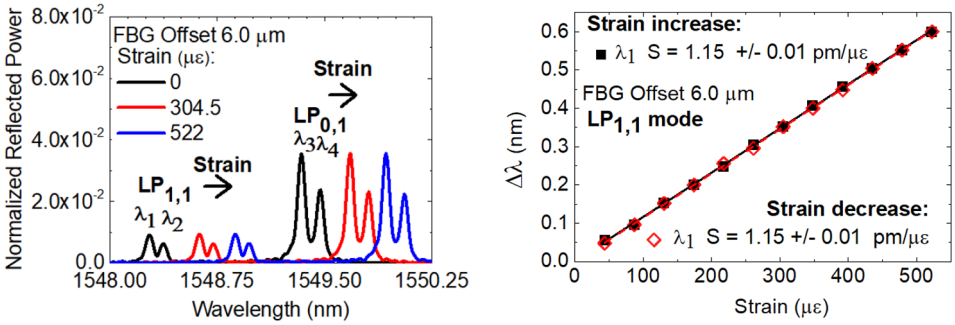

Fig. 7. Off-axis FBG with 6.0 μm offset from the core center: (a) reflection spectra for different strain values and (b) normalized wavelength shift (Δλ) as a function of strain.

Table 2
Strain sensitivities of the off-axis FBGs.

FBGs offset (μm)	Normalized wavelength shift (pm/με)			
	λ_1	λ_2	λ_3	λ_4
3.0	1.13 ± 0.01	1.13 ± 0.01	1.13 ± 0.01	1.13 ± 0.01
4.5	1.16 ± 0.01	1.16 ± 0.01	1.16 ± 0.01	1.16 ± 0.01
6.0	1.15 ± 0.01	1.15 ± 0.01	1.16 ± 0.01	1.15 ± 0.01

Table 3
Temperature sensitivities of the off-axis FBGs.

FBGs offset (μm)	Normalized wavelength shift (pm/°C)			
	λ_1	λ_2	λ_3	λ_4
3.0	12.04 ± 0.17	12.07 ± 0.17	11.99 ± 0.16	12.01 ± 0.16
4.5	11.94 ± 0.19	11.98 ± 0.19	11.94 ± 0.19	11.99 ± 0.19
6.0	11.70 ± 0.16	11.65 ± 0.19	11.75 ± 0.18	11.76 ± 0.19

majority of the RI modification was made in the cladding, leading to a smaller effective index modification, when compared with the off-axis FBGs with 3.0 and 4.5 μm offsets. The decay in the grating reflectivity is thus associated with the decrease in the RI modulation of the grating. The reason for this is that the thermally activated defects induced by the fs-laser FBG cladding inscription are annealed out, leading to a different annealing process due to other defects being present. To turn this off-axis FBG thermally stable it is necessary to perform a pre-annealing heat treatment at a higher temperature, typically at 700 °C [15]. However, with such treatment, the optical fiber becomes extremely brittle, which for strain and curvature measurements is a disadvantage.

F. Curvature measurements

The characterization of the off-axis FBGs was also performed in curvature and curvature direction angle θ.

The experimental characterization setup, presented in Fig. 9, contains a custom-made aluminum step-like cylinder with diameters between 0.04 m and 0.025 m, corresponding to curvatures in the range of

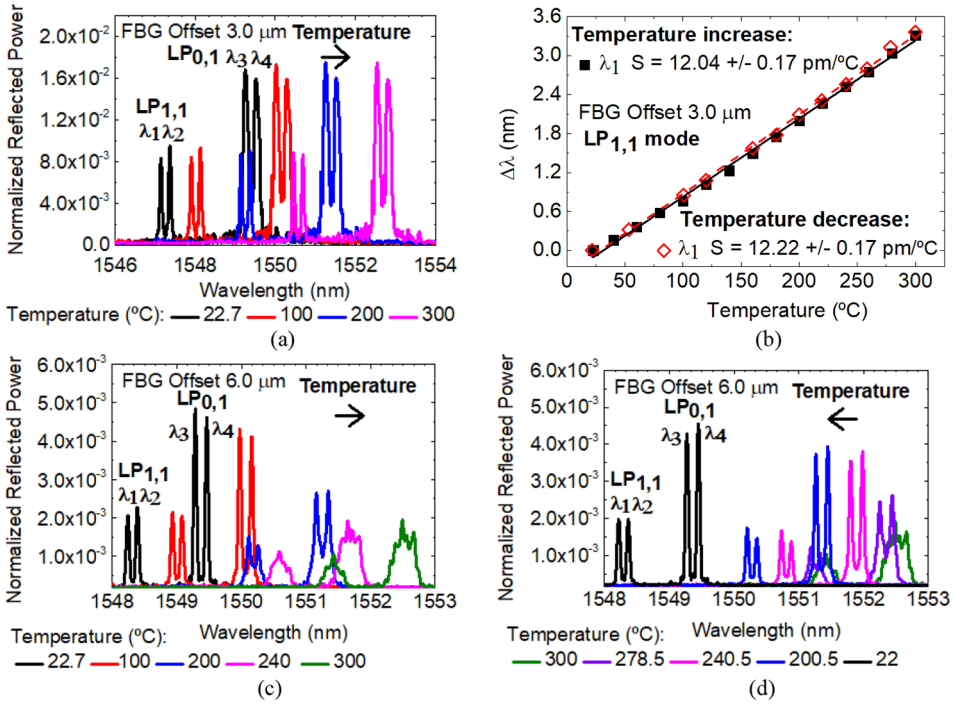

Fig. 8. Off-axis FBG with 3.0 μm offset: (a) reflection spectra for different temperature values and (b) normalized wavelength shift as a function of temperature; Off-axis FBG with 6.0 μm offset from the core center: (c) and (d) Reflection spectra for different temperature values.

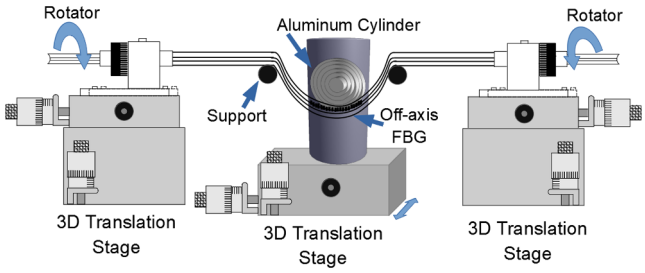

Fig. 9. Schematic diagram of the off-axis FBGs curvature setup.

50 to 80 m^{-1} respectively, which was mounted on a 3D translation stage. The fiber was placed around the cylinder with the section where the grating was inscribed (0.015 m) in the middle of the curvature radius. The ends of the fiber were then mounted on two rotary fiber holders which were fixed on a pair of 3D translation stages and separated by 0.4 m, with the aluminum cylinder between the two stages. The applied curvature can be changed by displacing the cylinder to the desired radius, and by moving the translation stages in order to fit the fiber to the cylinder. Before adjusting the fiber for a specific curvature radius, the bending orientation can be changed by simultaneously rotating the two rotary fiber holders, so that the optical fiber can be rotated as a whole without inducing twist.

Some aspects were considered during the curvature measurements: the curvature plane is defined as the plane passing through the center of the fiber and orthogonal to the optical table, the twisting strain was avoided, and the room temperature (~23 °C) was kept constant. The difficulty of ensuring the same fiber orientation when the different fibers were moved from the fabrication to the characterization setup lead to the assignment of a random initial orientation angle θ. This angle remained constant during curvature measurements. The curvature was always performed on the same plane. During the curvature direction angle θ characterization, the fiber was rotated an angle θ around its axis and 50 m^{-1} curvature was applied again. Depending on the defined angle for the curvature measurement, the off-axis FBGs will be stretched (when located at the outer side of the bend) or compressed (when located at the inner side of the bend).

Table 4
Curvature sensitivities of the off-axis FBGs.

FBGs offset (μm)	$LP_{1,1}$ mode	Normalized wavelength shift (pm/m^{-1})	Normalized reflected power variation ($1/m^{-1}$)
3.0	λ_1	7.48 ± 0.39	$(-1.370 \pm 0.065) \times 10^{-3}$
	λ_2	−1.81 ± 0.12	$(-0.898 \pm 0.142) \times 10^{-3}$
4.5	λ_1	7.53 ± 0.36	$(-0.739 \pm 0.064) \times 10^{-3}$
	λ_2	6.88 ± 0.22	$(0.768 \pm 0.054) \times 10^{-3}$
6.0	λ_1	8.25 ± 0.52	$(-0.049 \pm 0.004) \times 10^{-3}$
	λ_2	1.69 ± 0.07	$(0.023 \pm 0.001) \times 10^{-3}$

Fig. 10 shows the acquired reflection spectra of the $LP_{1,1}$ mode for the off-axis FBGs against the applied curvature at a random angle and the normalized reflected power variation (ΔNRP) as a function of curvature for the Bragg resonance (λ_1) of each off-axis FBG. When a curvature greater or equal to 50 m^{-1} was applied, the reflected optical power and the wavelength for both Bragg resonances of the $LP_{1,1}$ mode changed, as can be seen in Fig. 10 (a), (b) and (c).

The differences in the behavior of the intensity response of each resonance (see arrows in Fig. 10 (a – c)) are associated to the angle θ used to measure the curvature. Fig. 10 (d) shows the ΔNRP variation of the Bragg resonance (λ_1) of the $LP_{1,1}$ mode of each off-axis FBG. All devices display the same behavior for this resonance: the reflected power decreases as the curvature increases. Linear sensitivities of 1.37×10^{-3}, 7.39×10^{-4} and -4.94×10^{-5} $1/m^{-1}$ were obtained for the 3.0, 4.5 and 6.0 μm off-axis FBGs, respectively. Table 4 shows the curvature sensitivities of the off-axis FBGs tested. Maximum sensitivities were obtained for the off-axis FBGs with a 3.0 μm offset, due to the grating higher reflectivity. The sensitivity may be enhanced by a certain curvature direction angle θ, since the mode and off-axis FBG overlap is dependent on the curvature direction and the grating offset from the core center. Regarding the reflectivity of the off-axis FBGs, it was possible to conclude that the maximum grating reflectivity was achieved for the fabrication of the off-axis FBGs with a smaller offset from the core center. So, the sensitivities of the intensity to the curvature will be affected, decreasing for the off-axis FBGs with smaller reflectivity. The wavelength shifts of both Bragg resonances of the $LP_{1,1}$

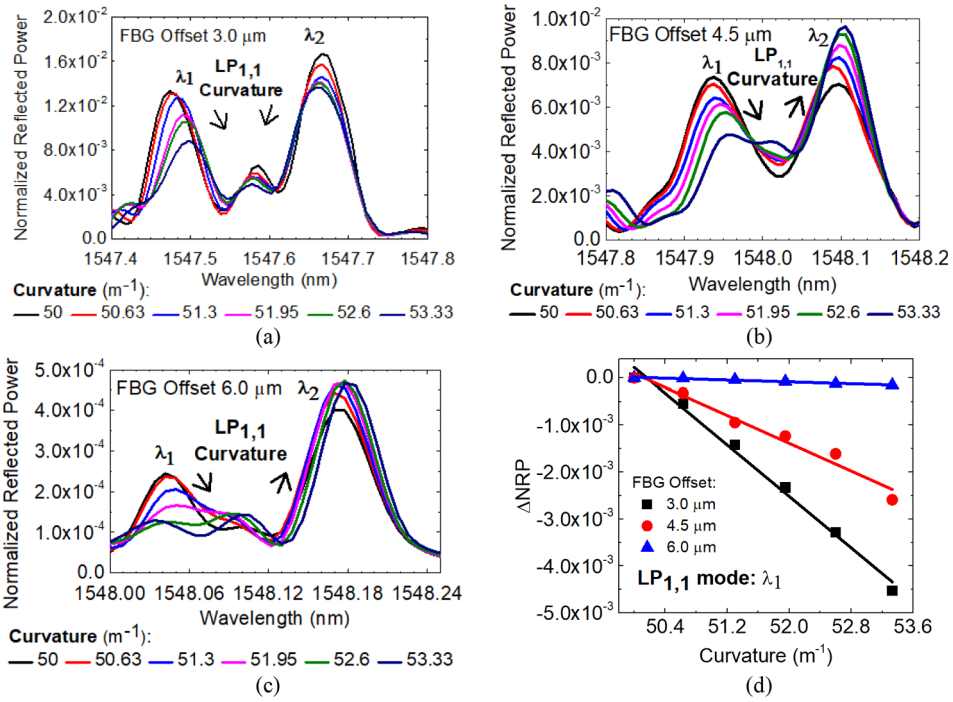

Fig. 10. Bragg resonances of the $LP_{1,1}$ mode (λ_1 and λ_2) of the three off-axis FBGs: reflection spectra under different curvature values at a random angle for the: (a) 3.0 μm, (b) 4.5 μm and (c) 6.0 μm off-axis FBGs, respectively. Also shown for the Bragg resonance of the $LP_{1,1}$ mode (λ_1) of each off-axis FBG: (d) the normalized reflected power variation as a function of curvature.

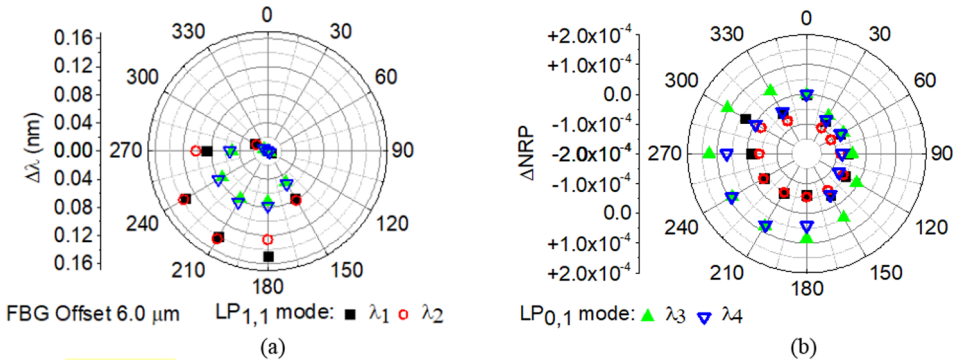

Fig. 11. Off-axis FBG with 6.0 μm offset: (a) normalized wavelength shift and (b) normalized reflected power variation as a function of the curvature direction angle θ under a curvature equal to 50 m^{-1}.

mode (λ_1 and λ_2) shown in Table 4 present curvature sensitivities in the order of few pm/m^{-1} that are not enough to detect the curvature response. Regarding, the $LP_{0,1}$ mode, it was also observed that both Bragg wavelengths are stable during the curvature measurement. For this mode, the reflected optical power shows fluctuations, resulting in a nonlinear response to the applied curvature.

To characterize the curvature direction angle, a curvature of 50 m^{-1} was chosen for the three off-axis FBGs. The normalized wavelength shift and the ΔNRP of the two Bragg resonances of the $LP_{1,1}$ and $LP_{0,1}$ mode were recorded in steps of 30° up to a complete rotation. Fig. 10 presents, in polar coordinates, the results achieved for the off-axis FBG with a 6.0 μm offset.

In Fig. 11 (a) and (b) it is clearly seen that each resonance presents a strong orientation dependence in wavelength and intensity depending on the angle θ. Analyzing the data from the three off-axis FBGs, it is visible that the response, both in wavelength and in intensity, to the curvature direction response increases with the increase of the offset distance. The observed wavelength response to the curvature's direction angle θ occurs because of the compression and stretching, resulting in a shift to shorter and longer wavelengths, respectively. From this information, it is possible to define the angle θ at which the off-axis FBGs were tested against the applied curvature. The angles used were 180°, 90° and 60° for the 3.0, 4.5 and 6.0 μm off-axis FBGs, respectively. Depending on the initially defined angle for the plane of curvature measurement, different curvature responses of each off-axis FBGs resonance are achieved, as observed in Fig. 11. The maximum sensitivity was obtained when the angle θ is parallel to the grating axis, and the minimum with the angle θ orthogonal to the grating. This is due to the asymmetric refractive index distribution induced by the fs-laser inscription and by the position of the grating inscription.

To compare our curvature sensitivity results with the literature, the ΔNRP values were converted to a logarithmic scale and presented in Table 5. A curvature sensitivity of 1.93 dB/m^{-1} (curvature range: 0 to 2.5 m^{-1}), and −0.21 dB/m^{-1} (curvature range: 25 to 80 m^{-1}) were reported for an off-axis ultraviolet written thin-core FBG, [3] and for a two-mode FBG fabricated by UV laser, [28], respectively. Compared to these curvature sensors based on the $LP_{1,1}$ mode resonance, the work presented here shows similar sensitivity for a curvature between 50 and 53.33 m^{-1}.

In summary, the $LP_{0,1}$ mode is not sensitive to curvature, while the optical power of the $LP_{1,1}$ mode is affected by it. The analysis of both modes allows a self-referenced optical power measurement. It was observed that the temperature changes do not affect the reflected optical power of the $LP_{0,1}$ mode for the 3.0 and 4.5 μm off-axis FBGs. This enables simultaneous measurement of curvature and temperature through the measurements of the intensity variations of the $LP_{1,1}$ mode and wavelength shift of the $LP_{0,1}$ mode, respectively.

Table 5
Curvature sensitivities (ΔNRP) of the off-axis FBGs.

FBGs offset (μm)	ΔNRP (dB/m^{-1}) $LP_{1,1}$ mode	
	λ_1	λ_2
3.0	−0.53 ± 0.04	−0.26 ± 0.04
4.5	−0.53 ± 0.06	0.40 ± 0.04
6.0	−1.33 ± 0.16	0.24 ± 0.02

4. Conclusions

The production of first order off-axis FBGs in an SMF-28e through fs-laser direct writing was demonstrated. When inscribing the grating with a lateral shift above 2.5 μm from the core center, we found that it is possible to fabricate a multimode section in the SMF-28e that can support two separate fiber modes ($LP_{0,1}$ and $LP_{1,1}$), each split into two degenerate polarization modes. The grating structures break the cylindrical symmetry of the fiber and introduce a birefringence on the order of 10^{-4}, which also depends on the grating inscription offset.

The characterization of three off-axis FBGs fabricated with 3.0, 4.5 and 6.0 μm offsets from the core center, was performed in strain, temperature, and curvature. The off-axis FBGs exhibit a similar strain and temperature sensitivities of ~1.14 pm/με, and ~12 pm/°C, respectively. For the off-axis FBG with a 6.0 μm offset, it was found that for temperatures above 240 °C the reflection spectra of the FBG becomes deformed and the two Bragg resonances poorly resolved, limiting the range of temperatures that can be sensed. The $LP_{0,1}$ and $LP_{1,1}$ modes of the three off-axis FBGs show a strong orientation dependence, in wavelength and intensity, to the plane of curvature. The Bragg resonance (λ_1) of the $LP_{1,1}$ mode present in the 3.0 μm offset off-axis FBG shows a maximum curvature sensitivity of 1.37 × 10^{-3} 1/m^{-1} at an angle of 180° for a curvature from 50 to 53.33 m^{-1}. The Bragg resonances of the $LP_{0,1}$ mode were not sensitive to curvature measurements. In addition, the different sensitivity of both modes to curvature enables the possibility to simultaneously measure curvature and temperature.

CRediT authorship contribution statement

Duarte Viveiros: Conceptualization, Methodology, Software, Validation, Formal analysis, Investigation, Data curation, Writing - original draft, Writing - review & editing. **Vítor A. Amorim:** Formal analysis, Writing - review & editing. **João M. Maia:** Formal analysis, Writing - review & editing. **Susana Silva:** Writing - review & editing. **Orlando Frazão:** Conceptualization, Writing - review & editing. **Pedro A.S. Jorge:** Writing - review & editing, Supervision, Writing - review & editing, Supervision. **Luís A. Fernandes:** Methodology, Software,

Formal analysis, Investigation, Writing - review & editing. **Paulo V.S. Marques:** Conceptualization, Writing - review & editing, Supervision, Conceptualization, Writing - review & editing, Supervision.

Declaration of Competing Interest

The authors declare that they have no known competing financial interests or personal relationships that could have appeared to influence the work reported in this paper.

Acknowledgments

This work was supported in part by the Ministry of Education and Science of the Portuguese Government under Grant SFRH/BD/110035/2015 and in part by Project “On Chip Whispering Gallery Mode Optical Microcavities For Emerging Microcontaminant Determination In Waters” - SAFE WATER, which is supported and co-funded by the European Commission, Directorate-General Communications Networks, Content and Technology (DG CONNECT) under the ERA-NET Cofund scheme - Horizon 2020 “Horizon 2020 – the Framework Programme for Research and Innovation (2014-2020)”.

References

[1] T. Erdogan, Fiber grating spectra, J. Light. Technol. 15 (1997) 1277–1294.
[2] Y. Wang, Z. Li, S. Liu, C. Fu, Z. Li, Z. Zhang, Y. Wang, J. He, Z. Bai, C. Liao, Parallel-integrated fiber Bragg gratings inscribed by femtosecond laser point-by-point technology, J. Light. Technol. 37 (2019) 2185–2193, https://doi.org/10.1109/JLT.2019.2899585.
[3] L. Zhang, X. Qiao, Q. Liu, M. Shao, Y. Jiang, D. Huang, Off-axis ultraviolet-written thin-core fiber Bragg grating for directional bending measurements, Opt. Commun. 410 (2018) 197–201, https://doi.org/10.1016/j.optcom.2017.09.061.
[4] D. Feng, X. Qiao, J. Albert, Off-axis ultraviolet-written fiber Bragg gratings for directional bending measurements, Opt. Lett. 41 (2016) 1201, https://doi.org/10.1364/ol.41.001201.
[5] S.J. Mihailov, C.W. Smelser, P. Lu, R.B. Walker, D. Grobnic, H. Ding, G. Henderson, J. Unruh, Fiber bragg gratings made with a phase mask and 800-nm femtosecond radiation, Opt. Lett. 28 (2003) 995–997, https://doi.org/10.1364/OL.28.000995.
[6] N. Jovanovic, A. Fuerbach, G.D. Marshall, M. Ams, M.J. Withford, Femtosecond Laser Micromachining 123 (2012), https://doi.org/10.1007/978-3-642-23366-1.
[7] S.J. Mihailov, Femtosecond Laser-Inscribed Fiber Bragg Gratings for Sensing Applications, Elsevier Inc., 2018. 10.1016/B978-0-12-803131-5.00006-4.
[8] C. Koutsides, K. Kalli, D.J. Webb, L. Zhang, Characterizing femtosecond laser inscribed Bragg grating spectra, Opt. Express. 19 (2011) 342, https://doi.org/10.1364/oe.19.000342.
[9] K. Chah, D. Kinet, C. Caucheteur, Negative axial strain sensitivity in gold-coated eccentric fiber Bragg gratings, Sci. Rep. 6 (2016) 1–6, https://doi.org/10.1038/srep38042.
[10] J.R. Grenier, L.A. Fernandes, P.R. Herman, Femtosecond laser inscription of asymmetric directional couplers for in-fiber optical taps and fiber cladding photonics, Opt. Express. 23 (2015) 16760–16771, https://doi.org/10.1364/OE.23.016760.
[11] J. Chen, Q. Liu, Z. He, S. Member, High-Resolution Simultaneous Measurement of Strain and Temperature Using π -Phase-Shifted FBG in Polarization Maintaining Fiber, 35 (2017) 4838–4844.
[12] L. Zhang, X. Qiao, W. Bao, Q. Liu, M. Shao, Strain and temperature discrimination using a fiber Bragg grating with off-axis inscription, Optik (Stuttg). 171 (2018) 941–946, https://doi.org/10.1016/j.ijleo.2018.06.128.
[13] X. Chen, C. Zhang, D.J. Webb, K. Kalli, G.D. Peng, Highly sensitive bend sensor based on bragg grating in eccentric core polymer fiber, IEEE Photonics Technol. Lett. 22 (2010) 850–852, https://doi.org/10.1109/LPT.2010.2046482.
[14] D. Su, X. Qiao, F. Chen, Q. Rong, Higher order coupling mode for orientation-dependent bend measurement using an off-axis FBG inscription over few-mode fiber, IEEE Sens. J. 19 (2019) 1368–1372, https://doi.org/10.1109/JSEN.2018.2881423.
[15] S.J. Mihailov, D. Grobnic, C. Hnatovsky, R.B. Walker, P. Lu, D. Coulas, H. Ding, Extreme environment sensing using femtosecond laser-inscribed fiber bragg gratings, Sensors (Switzerland) 17 (2017), https://doi.org/10.3390/s17122909.
[16] C. Caucheteur, T. Guo, J. Albert, Polarization-assisted fiber bragg grating sensors: tutorial and review, J. Light. Technol. 35 (2017) 3311–3322, https://doi.org/10.1109/JLT.2016.2585738.
[17] W. Tianshu, G. Yubin, Z. Xiaosu, M. Zhao, W. Ke, Simultaneous measurements of strain and temperature with dual fiber Bragg gratings for pervasive computing, SPCA 2006 2006 First Int. Symp. Pervasive Comput. Appl. Proc. (2007) 786–790. 10.1109/SPCA.2006.297530.
[18] Q. Rong, T. Guo, W. Bao, Z. Shao, G.D. Peng, X. Qiao, Highly sensitive fiber-optic accelerometer by grating inscription in specific core dip fiber, Sci. Rep. 7 (2017) 1–9, https://doi.org/10.1038/s41598-017-12322-6.
[19] K. Chah, D. Kinet, M. Wuilpart, P. Mégret, C. Caucheteur, Femtosecond-laser-induced highly birefringent Bragg gratings in standard optical fiber, Opt. Lett. 38 (2013) 594, https://doi.org/10.1364/ol.38.000594.
[20] D. Feng, W. Zhou, X. Qiao, J. Albert, Compact optical fiber 3D shape sensor based on a pair of orthogonal tilted fiber bragg gratings, Sci. Rep. 5 (2015) 1–7, https://doi.org/10.1038/srep17415.
[21] W. Bao, Q. Rong, F. Chen, X. Qiao, All-fiber 3D vector displacement (bending) sensor based on an eccentric FBG, Opt. Express. 26 (2018) 8619, https://doi.org/10.1364/oe.26.008619.
[22] Y. Zhao, C. Wang, G. Yin, B. Jiang, K. Zhou, C. Mou, Y. Liu, L. Zhang, T. Wang, Simultaneous directional curvature and temperature sensor based on a tilted few-mode fiber Bragg grating, Appl. Opt. 57 (2018) 1671, https://doi.org/10.1364/ao.57.001671.
[23] Y. Wang, S. Liu, Z. Li, C. Liao, Y. Wang, J. He, Z. Tan, K. Yang, J. Zhou, K. Guo, Femtosecond laser inscription of fiber Bragg grating in twin-core few-mode fiber for directional bend sensing, J. Light. Technol. 35 (2017) 4670–4676, https://doi.org/10.1109/jlt.2017.2750407.
[24] W. Bao, X. Qiao, Q. Rong, N. Hu, H. Yang, Z. Feng, M. Hu, Sensing characteristics for a fiber bragg grating inscribed over a fiber core and cladding, IEEE Photonics Technol. Lett. 27 (2015) 709–712, https://doi.org/10.1109/LPT.2015.2389860.
[25] F. Chen, D. Su, X. Qiao, Q. Rong, Compact vector bend sensor using dual-off-axis innermost cladding-type FBGs, IEEE Sens. J. 18 (2018) 7476–7480, https://doi.org/10.1109/JSEN.2018.2849360.
[26] Y.X. Jin, C.C. Chan, X.Y. Dong, Y.F. Zhang, Temperature-independent bending sensor with tilted fiber Bragg grating interacting with multimode fiber, Opt. Commun. 282 (2009) 3905–3907, https://doi.org/10.1016/j.optcom.2009.06.058.
[27] C. Wu, Z. Liu, K.M. Chung, M.L.V. Tse, F.Y.M. Chan, A.P.T. Lau, C. Lu, H.Y. Tam, Strong LP 01 and LP 11 mutual coupling conversion in a two-mode fiber Bragg grating, IEEE Photonics J. 4 (2012) 1080–1086, https://doi.org/10.1109/JPHOT.2012.2204735.
[28] H. Yu, W. Gao, X. Jiang, H. Guo, S. Jiang, Y. Zheng, On-line writing of fiber Bragg grating array on a two-mode optical fiber for sensing applications, Materials (Basel). 12 (2019), https://doi.org/10.3390/ma12081263.
[29] D. Viveiros, J.M. Maia, V.A. Amorim, P.A. Jorge, P. V. Marques, Fabrication of periodic structures in optical fibers by femtosecond laser micromachining for sensing applications, in: M.F.M. Costa (Ed.), SPIE 11207, Fourth Int. Conf. Appl. Opt. Photonics, Proc. of SPIE Vol. 11207 112070W-1, 2019: p. 69. 10.1117/12.2527261.
[30] L.A. Fernandes, O. Sezerman, G. Best, M.L. Ng, S. Kane, Direct writing of fiber optic components in photonic crystal fibers and other specialty fibers, Front. Ultrafast Opt. Biomed. Sci. Ind. Appl. XVI. 9740 (2016) 97400N. 10.1117/12.2213597.
[31] D. Choudhury, J.R. Macdonald, A.K. Kar, Ultrafast laser inscription: Perspectives on future integrated applications, Laser Photonics Rev. 8 (2014) 827–846, https://doi.org/10.1002/lpor.201300195.
[32] C. Chen, Foundations for guided-wave optics, John Wiley & Sons, 2006.
[33] Corning, Corning SMF-28e Product information, 2007.
[34] L.A. Fernandes, J.R. Grenier, P.V.S. Marques, J. Stewart Aitchison, P.R. Herman, Strong birefringence tuning of optical waveguides with femtosecond laser irradiation of bulk fused silica and single mode fibers, Light. Technol. J. 31 (2013) 3563–3569, https://doi.org/10.1109/JLT.2013.2284240.
[35] L.A. Fernandes, M. Becker, O. Frazão, K. Schuster, J. Kobelke, M. Rothhardt, H. Bartelt, J.L. Santos, P.V.S. Marques, Temperature and strain sensing with femtosecond laser written Bragg gratings in defect and nondefect suspended-silica-core fibers, IEEE Photonics Technol. Lett. 24 (2012) 554–556, https://doi.org/10.1109/LPT.2012.2183344.